Received: 30 November 2020 | Revised: 3 January 2021 | Accepted: 8 January 2021

DOI: 10.1002/hbm.25347

RESEARCH ARTICLE

WILEY

Distinct and temporally associated neural mechanisms underlying concurrent, postsuccess, and posterror cognitive controls: Evidence from a stop-signal task

Hengyi Cao[1,2,3,4] | Tyrone D. Cannon[4,5]

[1]Center for Psychiatric Neuroscience, Feinstein Institute for Medical Research, Manhasset, New York

[2]Division of Psychiatry Research, Zucker Hillside Hospital, Glen Oaks, New York

[3]Department of Psychiatry, Zucker School of Medicine at Hofstra/Northwell, Hempstead, New York

[4]Department of Psychology, Yale University, New Haven, Connecticut

[5]Department of Psychiatry, Yale University, New Haven, Connecticut

Correspondence
Hengyi Cao, MB, PhD, Center for Psychiatric Neuroscience, Feinstein Institute for Medical Research, 75-59 263 St, Glen Oaks, NY.
Email: hengyi.cao@hotmail.com

Funding information
Brain and Behavior Research Foundation, Grant/Award Number: 27068

Abstract

Cognitive control is built upon the interactions of multiple brain regions. It is currently unclear whether the involved regions are temporally separable in relation to different cognitive processes and how these regions are temporally associated in relation to different task performances. Here, using stop-signal task data acquired from 119 healthy participants, we showed that concurrent and poststop cognitive controls were associated with temporally distinct but interrelated neural mechanisms. Specifically, concurrent cognitive control activated regions in the cingulo-opercular network (including the dorsal anterior cingulate cortex [dACC], insula, and thalamus), together with superior temporal gyrus, secondary motor areas, and visual cortex; while regions in the fronto-parietal network (including the lateral prefrontal cortex [lPFC] and inferior parietal lobule) and cerebellum were only activated during poststop cognitive control. The associations of activities between concurrent and poststop regions were dependent on task performance, with the most notable difference in the cerebellum. Importantly, while concurrent and poststop signals were significantly correlated during successful cognitive control, concurrent activations during erroneous trials were only correlated with posterror activations in the fronto-parietal network but not cerebellum. Instead, the cerebellar activation during posterror cognitive control was likely to be driven secondarily by posterror activation in the lPFC. Further, a dynamic causal modeling analysis demonstrated that post-success cognitive control was associated with inhibitory connectivity from the lPFC to cerebellum, while excitatory connectivity from the lPFC to cerebellum was present during posterror cognitive control. Overall, these findings suggest dissociable but temporally related neural mechanisms underlying concurrent, postsuccess, and posterror cognitive control processes in healthy individuals.

KEYWORDS
cerebellum, cingulo-opercular network, cognitive control, fronto-parietal network, posterror, poststop

1 | INTRODUCTION

Successful cognitive control in humans depends on consistently and effectively monitoring performance to adjust one's thoughts and behaviors. While the dorsal anterior cingulate cortex (dACC) has been the major focus of cognitive control in the literature (M. M. Botvinick, Cohen, & Carter, 2004; Carter et al., 1998; Carter & van Veen, 2007; Kerns et al., 2004), other areas such as ventro- and dorsolateral prefrontal cortex (vlPFC, dlPFC), anterior insula, posterior cerebellum, inferior parietal lobule (IPL), supplementary motor area (SMA), and thalamus have also been shown to be involved in performance monitoring (Ide & Li, 2011; Kerns et al., 2004; Menon, Adleman, White, Glover, & Reiss, 2001; Taylor, Stern, & Gehring, 2007). Part of these areas constitute two fundamental cognitive control networks in humans generally referred to as the cingulo-opercular network and the fronto-parietal network (Dosenbach, Fair, Cohen, Schlaggar, & Petersen, 2008). Notably, dysfunction in both networks, together with other regions such as cerebellum, has been implicated in a variety of common mental disorders including schizophrenia (Becerril & Barch, 2013; H. Cao et al., 2018; H. Cao et al., 2019), obsessive compulsive disorder (Anticevic et al., 2014; Carlisi et al., 2017; Sha et al., 2020), autism (Carlisi et al., 2017; Ito et al., 2017; Lynch et al., 2017), and attention deficit hyperactivity disorder (Duan et al., 2018; Mostert et al., 2016). Such dysfunction has been hypothesized to be a core contributor to cognitive deficits in these disorders (H; Cao & Cannon, 2019), making the study of neural mechanisms underlying cognitive control processes particularly interesting in both cognitive and clinical neuroscience.

An unsolved question, however, is whether the functional engagement of relevant regions during a cognitive control task has different meanings in support of goal-directed behaviors. Specifically, a conflict during the task may generate neural activities associated with two consecutive cognitive processes: activities facilitating the detection and monitoring of concurrently unexpected information, and activities aiming at solving such unexpected input in order to prevent behavior from derailing (Carter & van Veen, 2007). To date, little has been known as which brain regions are involved in each of these two processes. A series of early studies focusing on the dACC and lPFC have suggested distinct roles of these two areas during cognitive control (M. M. Botvinick et al., 2004; Carter et al., 1998; Carter & van Veen, 2007; Garavan, Ross, Murphy, Roche, & Stein, 2002; Kerns et al., 2004; MacDonald 3rd, Cohen, Stenger, & Carter, 2000). In particular, conflict-related activity in the dACC has been shown to significantly predict lPFC activity in the following nonconflict trials (Kerns et al., 2004), suggesting that the function of dACC is more specific to concurrent cognitive control, while the function of lPFC is more specific to postconflict cognitive control. However, except for dACC and lPFC, little research has been performed to investigate the roles of other regions activated during a cognitive control task. Therefore, the first aim of this study was to investigate whether activations of different regions generally signify a "detection" signal or an "adaption" signal, and how the regions involved in temporally separate cognitive processes are interrelated over time in orchestrating cognitive control behaviors.

While unsuccessful cognitive control leads to errors in behaviors, the neural mechanisms underlying successful and unsuccessful cognitive controls are considered to be dissociable (Garavan, Ross, Kaufman, & Stein, 2003; Garavan et al., 2002; Hendrick, Ide, Luo, & Li, 2010; Mathalon, Whitfield, & Ford, 2003; Y. Zhang et al., 2017). The distinction in neural mechanism seems to be particularly represented by the differential associations between activities of concurrent cognitive control and those of postconflict/stop cognitive control. For instance, Hendrick et al. (2010) reported that the activations of lPFC during posterror trials and postsuccess trials are likely to be triggered by different preceding activations. This implies that the brain is likely to dynamically change its connectivity patterns to subserve posterror cognitive control in order for behavioral adjustment. Based on this assumption, the second aim of this study was therefore to examine whether and how the connectivity patterns are different between postsuccess trials and posterror trials among regions activated during a cognitive control task.

Here, we sought to investigate these questions in a sample of 119 healthy subjects who underwent functional magnetic resonance imaging (fMRI) scans with a stop-signal task. The trials were separated by whether they were currently eliciting a stop signal or immediately followed a stop signal, and by whether the task response was correct or not, thereby generating 2×2 contrasts measuring concurrent correct cognitive control, concurrent incorrect cognitive control, poststop cognitive control for prior success, and poststop cognitive control for prior error, respectively. We examined the neural correlates of these contrasts and investigated how the brain regions activated during different contrasts were temporally associated. Based on these findings, we further used dynamic causal modeling (DCM) to examine how the effective connectivity between these regions were modulated by different task conditions. We hypothesized the presence of distinct but temporally associated brain regions in relation to concurrent and poststop monitoring, and different connectivity patterns between correct and erroneous trials.

2 | MATERIALS AND METHODS

2.1 | Subjects and paradigm

This study included 119 healthy subjects (age 31.78 ± 8.83 years, 64 males) drawn from the Consortium for Neuropsychiatric Phenomics (CNP) dataset (https://openneuro.org/datasets/ds000030). All participants provided written informed consent following procedures approved by the Institutional Review Board at University of California, Los Angeles. For details of this public dataset see previous publications (Gorgolewski, Durnez, & Poldrack, 2017; Poldrack et al., 2016). In particular, all subjects in the present sample completed a stop-signal task. During the task, the subjects were asked to press either left or right button according to the directionality of the arrows shown on the screen, but to withhold the response when an arrow was followed by a "stop-signal" tone. The delay between the arrow and the "stop-signal" tone ("stop-signal delay," SSD) was

tailored for each individual to ensure that all subjects successfully inhibited on approximately half of the "stop" trials. In case of a successful inhibition, the SSD would be increased, while an unsuccessful inhibition would lead to a decrease of SSD. The task consisted of a total of 96 "go" trials and 32 "stop" trials, with each arrow lasting for 1 s and jittered interstimulus interval ranging between 0.5 and 4 s.

2.2 | Data acquisition

The fMRI data were acquired from the 3T Siemens Trio scanners using echo-planar imaging (EPI) sequence with the following parameters: TR = 2 s, TE = 30 ms, flip angle = 90°, matrix = 64 × 64, FOV = 192 mm, slice thickness = 4 mm, and 34 slices. In addition, high-resolution T1-weighted anatomical images were acquired using the following sequence: TR = 1.9 s, TE = 2.26 ms, FOV = 250 mm, matrix = 256 × 256, slice thickness = 1 mm, and 176 slices.

2.3 | Behavioral data processing

To ensure poststop cognitive control effects during the task, we first computed "go"-trial reaction times (RTs) immediately following "go" trials, "stop" trials, correct trials, and erroneous trials. We expected to see significantly slower RTs for trials following stops and errors compared with those following go and correct responses.

2.4 | Imaging data processing

Data preprocessing was performed using the standard pipeline implemented in the Statistical Parametric Mapping software (SPM12, https://www.fil.ion.ucl.ac.uk/spm/). In brief, fMRI images were slice-time corrected, realigned for head motion, registered to the individual T1-weighted structural images, and spatially normalized to the Montreal Neurological Institute (MNI) template. Finally, the normalized images were spatially smoothed with an 8 mm full-width at half-maximum (FWHM) Gaussian kernel. The preprocessed data were then scrutinized for head motion. In particular, we calculated the frame-wise displacement (FD) for each individual based on the previous definition (Power et al., 2014). Two subjects had mean FD >0.26 mm and were excluded from the further analysis. The threshold was chosen as the mean FD of all subjects plus three times the standard deviation.

We modeled the following task conditions for each subject: successful "go" condition ("Hit"), unsuccessful "go" condition ("Miss"), successful "stop" condition (correct rejection, "CR"), and unsuccessful "stop" condition (false alarm, "FA"). For the "Hit" condition, we further modeled three subconditions: trials preceded by successful "go" ("post-Hit"), trials preceded by successful "stop" ("post-CR"), and trials preceded by unsuccessful "stop" ("post-FA"). Notably, only approximately 2% of total "go" trials (∼1 trial per subject) were in the "Miss" condition. Due to the extremely small number of trials, the "Miss" condition was not considered in the subsequent activation and connectivity analyses. The "CR" and "FA" conditions comprised 49% and 51% of the total "stop" trials, respectively.

The first-level general linear model was performed on the preprocessed images where all task conditions were included as regressors after convolved with the canonical hemodynamic response function at each trial. In addition, the 24 head motion parameters (i.e., the 6 rigid-body parameters generated from the realignment step, their first derivatives, and the squares of these 12 parameters) and the FD at each time point were also included in the model to mitigate potential head motion effects. The images were then high-pass filtered at 0.008 Hz. We subsequently computed two sets of contrasts for each subject, detailed as below.

1. To assess concurrent cognitive control: "CR" + "FA" vs. "Hit" (modeling overall concurrent cognitive control), "CR" vs. "Hit" (modeling successful concurrent cognitive control), and "FA" vs. "Hit" (modeling unsuccessful concurrent cognitive control);
2. To assess poststop cognitive control: "post-CR" + "post-FA" vs. "post-Hit" (modeling overall poststop cognitive control), "post-CR" vs. "post-Hit" (modeling poststop cognitive control for prior success), and "post-FA" vs. "post-Hit" (modeling poststop cognitive control for prior error).

These computed contrast images were then entered into random-effects second-level analyses to examine significantly activated regions for each contrast. Statistical significance was determined after correction for family-wise error (FWE) across all voxels in the brain. For significantly activated regions, percent signal changes were extracted and Pearson correlations were performed to investigate the relationships between signal changes during concurrent cognitive control and those during poststop cognitive control. The analysis was performed for CR/post-CR and FA/post-FA separately. p values were reported after FWE correction across all performed correlation analyses (see Section 3).

2.5 | Dynamic causal modeling

Based on the observed correlations between concurrent and poststop activations (see Section 3 and Figures 2 and 3), we further investigated how the effective connectivity between lPFC and cerebellum was modulated by poststop trials. Here, nodes were defined by two steps. First, we extracted the activated clusters from the group-level contrast maps, thresholded at p_{FWE} <.05. The extracted clusters were then superimposed on the anatomical masks of relevant regions defined by the Automated Anatomical Labeling atlas. The overlaps between the functional clusters and the anatomical masks were subsequently extracted as group-level ROIs. Second, for each individual, we searched for the peak activation voxels within the group-level ROIs. A sphere was subsequently drawn with a 5 mm radius centering on each peak voxel, and the time series were extracted from the derived spheres. The time series were further corrected for 24 head motion parameters and FD, and were used for the DCM analysis.

DCM is a Bayesian statistic-based approach to examine how a brain region intrinsically exerts influence over another and how such influence is modulated by an experimental condition (Friston, Harrison, & Penny, 2003; Stephan et al., 2010; Zeidman et al., 2019). In particular, DCM models three brain dynamics: (1) the intrinsic effective connectivity between brain regions; (2) the driving input of an experimental condition on brain regions themselves; and (3) the modularity effect of an experimental condition on the coupling between brain regions. Here, we considered bidirectional intrinsic connectivity between the two regions. In terms of the correlation results, driving input was modeled to the lPFC and modulatory effect was modeled to the connectivity from lPFC to cerebellum during post-FA. During post-CR, three possibilities were considered for driving input, namely, input to the lPFC, input to the cerebellum, and input to both regions. Similarly, three possibilities were considered for modulatory effect (i.e., effect on connectivity from lPFC to cerebellum, effect on connectivity from cerebellum to lPFC, and effect on both directions). This generated a total of $3 \times 3 = 9$ models for each individual. An illustration for all defined models is present in Figure 4a.

The inference of optimal model structure was performed using random-effects Bayesian model selection (BMS), which is based on the comparison of model evidence that represents a trade-off between model accuracy and model complexity, given the present data (Stephan et al., 2010; Stephan, Penny, Daunizeau, Moran, & Friston, 2009). Under the framework of BMS, the optimal model is determined by the protected exceedance probability, which quantifies the probability that one model is more likely than the others in the comparison set, corrected for an overconfidence bias (Rigoux, Stephan, Friston, & Daunizeau, 2014). After the optimal model structure was determined, Bayesian model averaging (BMA) was used to calculate group-level model parameters. Since the optimal model structure for a single individual may differ from that at the group level, the BMA is an effective approach to account for heterogeneity in model structures between individuals and provides weighted averages of each model parameter based on the entire comparison set, where the weights are decided by the posterior probability of each model (Penny et al., 2010; Stephan et al., 2010). For the derived intrinsic connectivity and driving inputs, one-sample *t* tests were subsequently performed to investigate whether they were significantly different from zero. For the derived modularity effects, paired t tests were employed to investigate whether they were significantly different between post-CR and post-FA. Significance was determined after FWE correction across the examined DCM parameters.

3 | RESULTS

3.1 | Task performance

As expected, significant poststop and posterror slow-down was evident during the task. Specifically, the mean RT for the "poststop" trials was 520 ms, compared to 479 ms for the "postgo" trials (paired *t* test p <.001). Similarly, the mean RTs for the "posterror" and "postsuccess" trials were 518 ms and 501 ms, respectively (paired *t* test p <.001), suggesting strong effects for poststop and posterror cognitive controls.

3.2 | Activation maps

3.2.1 | Concurrent cognitive control

For overall concurrent cognitive control ("CR" + "FA" vs. "Hit"), successful concurrent cognitive control ("CR" vs. "Hit"), and unsuccessful concurrent cognitive control ("FA" vs. "Hit"), significant activations were observed in the cingulo-opercular network, in particular the dACC, insula, and thalamus. In addition to the regions traditionally defined as part of the cingulo-opercular network (Dosenbach et al., 2008), significant activations were also observed in the superior temporal gyrus (STG), secondary motor areas including SMA and premotor cortex, and in part of the visual cortex including the cuneus and lingual gyrus (all p_{FWE} <.05, Figure 1a). In contrast, regions in the fronto-parietal network and cerebellum were not activated during concurrent cognitive control.

3.2.2 | Poststop cognitive control

In terms of poststop cognitive control, we observed completely different activation patterns compared with concurrent cognitive control. Specifically, the fronto-parietal network including the dlPFC, vlPFC, and posterior parietal cortex was significantly activated for overall poststop cognitive control ("post-CR" + "post-FA" vs. "post-Hit"), poststop cognitive control for prior success ("post-CR" vs. "post-Hit"), and poststop cognitive control for prior error ("post-FA" vs. "post-Hit"). In addition, the posterior cerebellum was also significantly activated during poststop cognitive control (all p_{FWE} <.05, Figure 1b), and the activation was chiefly located at the fronto-parietal system of cerebellum according to a previous parcellation (Ji et al., 2019). In contrast, no activation in the cingulo-opercular network was observed. Details on activated peak voxels for all contrasts are listed in Table 1.

3.3 | Associations between concurrent and poststop activations

The activation results clearly showed six major clusters for concurrent cognitive control, namely, the dACC, STG, insula, thalamus, cuneus, and SMA, and three major clusters for poststop cognitive control, namely, the cerebellum, lPFC, and IPL. To investigate whether and how the activations during concurrent and poststop cognitive controls were related, we calculated percent signal changes for each of the nine regions by drawing a 5 mm radius sphere around the peak voxels in each cluster, and examined the correlations of signal changes between concurrent and poststop control regions. We found that for correct trials (CR and post-CR), concurrent signal changes were

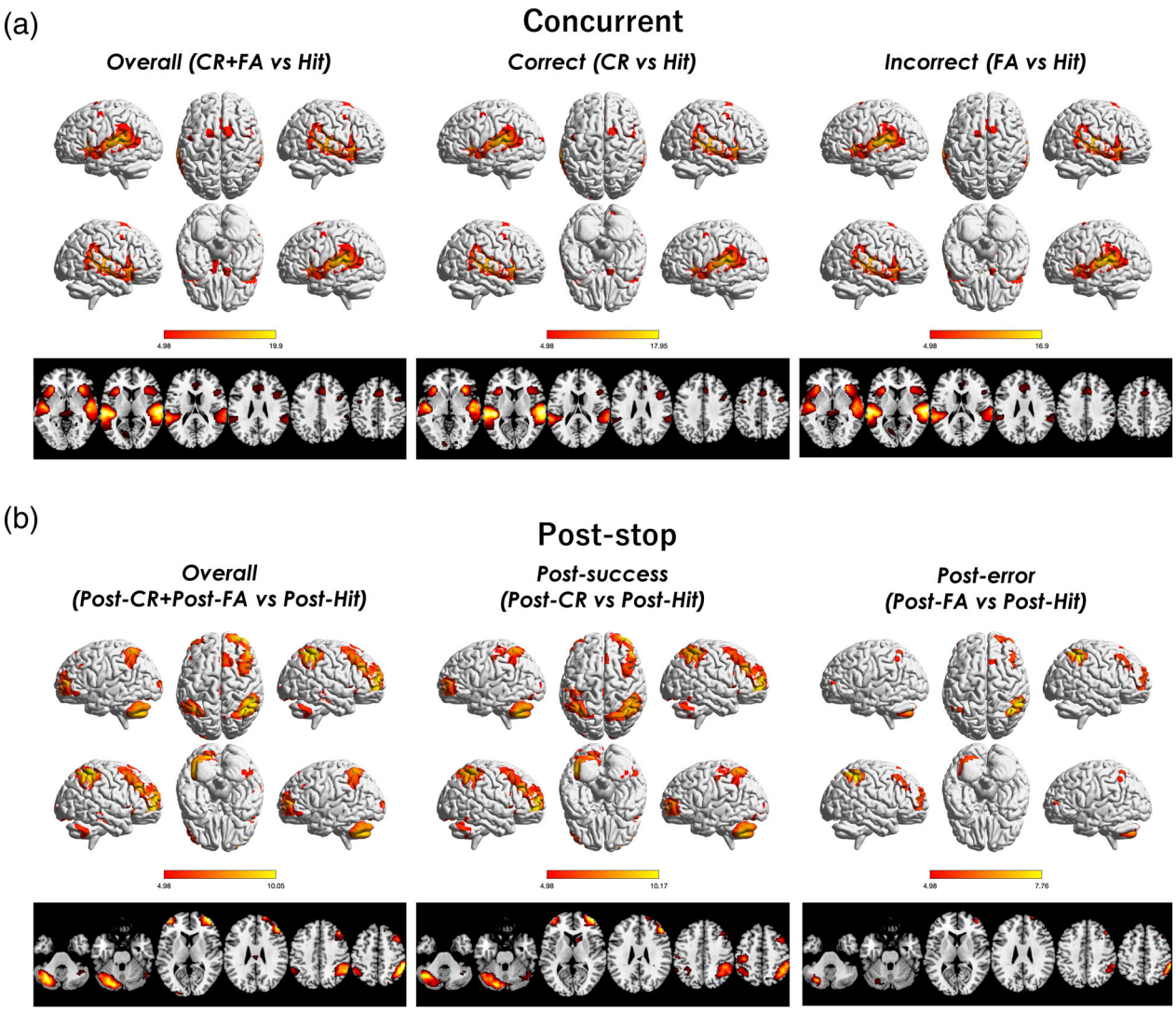

FIGURE 1 Activation maps for the modeled contrasts in the stop-signal task. (a) For concurrent cognitive control, significant activations were shown in the cingulo-opercular network, in particular the anterior cingulate cortex, insula, and thalamus, as well as the superior temporal gyrus, supplementary motor area and visual cortex. (b) In contrast, poststop cognitive control was associated with significant activations in the fronto-parietal network and cerebellum. The maps are thresholded at voxel-level p_{FWE} <.05 across the whole brain

significantly correlated with poststop signal changes in all three post-activated regions (R >.26, P_{FWE} <.05, corrected across 6 × 3 = 18 comparisons, Figure 2). However, for incorrect trials (FA and post-FA), concurrent signal changes were only correlated with poststop signal changes in the lPFC and IPL (R >.33, P_{FWE} <.01, Figure 3), while no correlations of concurrent signal changes with cerebellum were observed. These findings suggest that postsuccess and posterror activations in the cerebellum are possibly related to distinct neural mechanisms.

Given that posterror activation in the cerebellum was not related to any of concurrent activations, we hypothesized that the detected cerebellar activation may be driven secondarily by other regions during posterror cognitive control. To test this, we further correlated signal changes in the lPFC and IPL with those in the cerebellum. The result demonstrated a significant correlation between lPFC and cerebellum (R = .43, P_{FWE} <.001, Figure 3) and trend-level between IPL and cerebellum (R = .18, P_{FWE} = .05), suggesting that the posterror cerebellar activation is mainly related to posterror activation in the lPFC.

3.4 | Dynamic causal modeling

According to the results from the correlation analyses, we used DCM to estimate how effective connectivity between lPFC and cerebellum was differentially modulated by postsuccess and posterror cognitive controls. The BMS identified a clearly winning model with the protected exceedance probability of 0.73. Specifically, the winning model demonstrated remarkable differences in model structure between post-CR and post-FA (Figure 4b). In contrast to post-FA which input to the lPFC and affected top-down connectivity from lPFC to cerebellum, the post-CR condition exerted its driving input to the cerebellum and modulated connectivity of both directions (from lPFC to

TABLE 1 Full list of activated peak voxels for all examined contrasts in the stop-signal task, thresholded at p_{FWE} <.05 cross all voxels in the brain

Cluster size	Peak voxel region	MNI coordinates (*x*, *y*, *z*)			*T* value	p_{FWE}
Overall concurrent cognitive control (CR + FA > Hit)						
9,307	R. Superior temporal gyrus	62	−22	6	19.76	<.001
	R. Insula	52	−10	0	15.92	<.001
6,831	L. Superior temporal gyrus	−60	−30	10	19.90	<.001
	L. Transverse temporal gyrus	−44	−30	8	17.55	<.001
	L. Insula	−48	−14	0	16.08	<.001
2,211	R. Anterior cingulate cortex	8	18	40	9.97	<.001
	R. Supplementary motor area	14	8	66	8.46	<.001
102	L. Premotor cortex	−40	−2	46	6.69	<.001
816	L. Thalamus	−4	−30	−6	8.57	<.001
	R. Thalamus	14	−24	−8	7.86	<.001
112	R. Lentiform nucleus	12	8	−10	7.51	<.001
330	L. Cuneus	−8	−76	12	6.52	<.001
	L. Posterior cingulate cortex	−16	−68	6	6.35	<.001
	L. Lingual gyrus	−20	−48	−4	5.56	<.001
43	L. Precuneus	−8	−46	50	6.41	<.001
99	R. Parahippocampal gyrus	24	−52	2	6.30	<.001
60	L. Supplementary motor area	−12	2	72	5.66	.004
55	L. Lentiform nucleus	−12	6	0	5.49	.007
3	R. Posterior cingulate cortex	14	−66	10	5.15	.027
2	L. Inferior parietal lobule	−64	−30	36	5.11	.031
5	R. Lingual gyrus	18	−42	−8	5.07	.036
3	R. Precuneus	16	−68	36	5.05	.039
Successful concurrent cognitive control (CR > Hit)						
7,947	R. Superior temporal gyrus	64	−22	6	17.95	<.001
4,166	L. Superior temporal gyrus	−58	−32	10	17.68	<.001
	L. Transverse temporal gyrus	−42	−28	8	17.58	<.001
1,262	L. Lentiform nucleus	−32	24	0	13.49	<.001
	L. Insula	−32	18	10	11.41	<.001
893	R. Anterior cingulate cortex	6	18	44	8.31	<.001
	R. Supplementary motor area	16	6	66	7.63	<.001
110	L. Inferior frontal gyrus	−40	−2	46	7.25	<.001
223	L. Cuneus	−10	−94	−2	7.09	<.001
78	R. Lingual gyrus	18	−88	−6	6.29	<.001
151	L. Thalamus	−12	−28	−6	6.19	<.001
	R. Thalamus	6	−22	−4	5.98	<.001
32	L. Precuneus	−6	−48	52	5.93	.001
66	L. Anterior cingulate cortex	−2	34	20	5.51	.007
9	L. Middle frontal gyrus	−40	12	24	5.19	.023
Unsuccessful concurrent cognitive control (FA > Hit)						
6,464	L. Superior temporal gyrus	−62	−24	10	16.63	<.001
	L. Transverse temporal gyrus	−44	−30	8	14.14	<.001
7,875	R. Superior temporal gyrus	64	−22	8	16.90	<.001
	R. Insula	34	26	0	13.53	<.001
1796	R. Anterior cingulate cortex	8	18	40	8.20	<.001
	L. Anterior cingulate cortex	−4	24	24	7.36	<.001
	L. Supplementary motor area	−2	12	52	7.88	<.001

TABLE 1 (Continued)

Cluster size	Peak voxel region	MNI coordinates (x, y, z)			T value	p_{FWE}
74	R. Middle frontal gyrus	42	6	42	6.33	<.001
819	L. Thalamus	−4	−30	−6	8.73	<.001
	R. Thalamus	10	−26	−8	8.52	<.001
313	L. Posterior cingulate cortex	−16	−66	6	6.69	<.001
	L. Cuneus	−8	−76	12	6.33	<.001
	L. Parahippocampal gyrus	−20	−50	−2	6.15	<.001
106	R. Parahippocampal gyrus	22	−54	2	6.67	<.001
42	R. Lentiform nucleus	12	6	−10	6.14	<.001
61	L. Inferior frontal gyrus	−44	12	22	5.86	.002
19	R. Posterior cingulate cortex	12	−66	12	5.42	.009
11	R. Lingual gyrus	18	−40	−6	5.40	.010
3	L. Precuneus	−8	−46	50	5.15	.026
8	L. Lentiform gyrus	−10	8	−4	5.08	.033
1	R. Precuneus	18	−68	36	4.97	.049
Overall poststop cognitive control (post-CR + post-FA vs. post-Hit)						
2,168	*R. inferior* parietal lobule	44	−46	58	10.05	<.001
3,077	R. Middle frontal gyrus	38	54	−4	9.78	<.001
	R. Superior frontal gyrus	46	34	32	9.44	<.001
2,961	L. Cerebellum, crus 1	−18	−80	−28	9.48	<.001
	L. Cerebellum, crus 1	−36	−70	−42	9.11	<.001
687	L. Middle frontal gyrus	−40	52	8	8.55	<.001
	L. Superior frontal gyrus	−34	60	0	7.16	<.001
694	L. Inferior parietal lobule	−38	−54	60	8.51	<.001
140	L. Middle occipital gyrus	−22	−98	4	6.98	<.001
229	R. Superior frontal gyrus	6	26	66	6.95	<.001
43	R. Inferior frontal gyrus	52	20	−6	6.44	<.001
340	R. Cerebellum, crus 1	34	−58	−42	6.35	<.001
30	R. Middle temporal gyrus	66	−30	−10	6.02	.001
80	R. Middle cingulate cortex	2	−24	−20	5.72	.003
7	L. Inferior frontal gyrus	−50	36	−10	5.48	.007
11	R. Caudate	14	10	16	5.43	.009
15	R. Inferior temporal gyrus	58	−24	−24	5.35	.012
19	R. Middle occipital gyrus	28	−94	−2	5.20	.022
3	R. Superior parietal lobule	6	−68	62	5.11	.030
4	R. Cerebellum, lobule 6	28	−60	−32	5.11	.031
2	R. Inferior temporal gyrus	60	−34	−22	5.09	.032
1	R. Cuneus	18	−100	4	5.00	.045
Poststop cognitive control for prior success (post-CR vs. post-Hit)						
2,725	R. Middle frontal gyrus	38	52	−4	10.17	<.001
	R. Superior frontal gyrus	46	34	30	9.48	<.001
3,092	L. Cerebellum, crus 2	−42	−60	−40	9.54	<.001
	L. Cerebellum, crus 1	−18	−80	−28	9.50	<.001
	L. Cerebellum, crus 1	−14	−74	−32	8.97	<.001
2,995	R. Inferior parietal lobule	42	−46	58	9.33	<.001
1746	L. Postcentral gyrus	−36	−28	54	8.33	<.001
	L. Superior parietal lobule	−34	−58	60	8.19	<.001
	L. Inferior parietal lobule	−40	−50	58	8.17	<.001

(Continues)

TABLE 1 (Continued)

Cluster size	Peak voxel region	MNI coordinates (*x*, *y*, *z*)			*T* value	p_{FWE}
698	L. Superior frontal gyrus	−34	60	0	8.27	<.001
	L. Middle frontal gyrus	−38	52	6	7.89	<.001
301	R. Caudate	10	10	10	6.78	<.001
45	R. Superior frontal gyrus	6	26	64	6.24	<.001
372	R. Cerebellum, crus 1	50	−60	−30	6.24	<.001
	R. Cerebellum, lobule 8	34	−58	−44	6.20	<.001
29	R. Cerebellum, lobule 6	26	−46	−22	5.84	.002
21	R. Inferior frontal gyrus	52	20	−6	5.84	.002
52	R. Posterior cingulate cortex	2	−28	24	5.82	.002
4	R. Cerebellum, vermis 6	4	−64	−20	5.32	.015
3	L. Insula	−50	−18	22	5.29	.016
3	L. Inferior occipital gyrus	−44	−82	−14	5.28	.017
3	R. Inferior temporal gyrus	58	−56	−18	5.28	.017
7	L. Caudate	−16	6	14	5.26	.019
11	R. Lingual gyrus	6	−96	−4	5.22	.021
6	R. Middle occipital gyrus	16	−100	12	5.15	.028
17	L. Middle occipital gyrus	−32	−94	4	5.14	.029
1	L. Lentiform nucleus	−24	8	2	5.04	.041
1	R. Medial frontal gyrus	22	46	14	5.01	.046
1	R. Lentiform gyrus	22	10	−6	5.00	.049
Poststop cognitive control for prior failure (post-FA vs. *post-Hit)*						
704	R. Inferior parietal lobule	56	−44	40	7.76	<.001
636	L. Cerebellum, crus 2	−28	−72	−40	7.14	<.001
434	R. Superior frontal gyrus	40	54	14	6.45	<.001
259	R. Middle frontal gyrus	42	50	6	6.22	<.001
21	L. Inferior parietal lobule	−40	−56	50	5.80	.002
24	R. Superior frontal gyrus	16	22	60	5.57	.005
9	L. Middle frontal gyrus	−42	52	8	5.30	.014
13	L. Inferior parietal lobule	−54	−52	48	5.26	.016
1	L. Cerebellum, crus 1	−46	−64	−32	4.96	.049

cerebellum and from cerebellum to lPFC). Importantly, the connectivity from lPFC to cerebellum was positively modulated (excited) during post-FA but negatively modulated (inhibited) during post-CR (Figure 4b,c).

4 | DISCUSSION

Using a stop-signal task, this study demonstrated that neural mechanisms underlying concurrent and poststop cognitive controls were both temporally dissociable and related. Specifically, concurrent cognitive control was associated with activations in the cingulo-opercular network (including the dACC, insula, and thalamus), together with STG, secondary motor areas and visual cortex; while poststop cognitive control was associated with activations in the fronto-parietal network (including the lPFC and IPL), as well as cerebellum. Importantly, while concurrent and poststop signals were significantly correlated during successful cognitive control, concurrent activations during unsuccessful cognitive control were only correlated with posterror activations in the lPFC and IPL but not cerebellum. Instead, the cerebellar activation during posterror cognitive control was likely to be driven by increased excitatory connectivity from lPFC to cerebellum. Together, the present data suggest distinct but temporally associated neural mechanisms underlying concurrent, postsuccess, and posterror cognitive control processes in healthy individuals.

Although the two cognitive control networks in humans (cingulo-opercular and fronto-parietal) have been established for a decade (Dosenbach et al., 2008), whether and how regions in these networks are related to temporally different cognitive control processes remain unclear. The hypothesis that the preceding activity of dACC drives successive activation in the lPFC to solve an existing conflict has suggested potentially dissociable functions for (at least some) regions

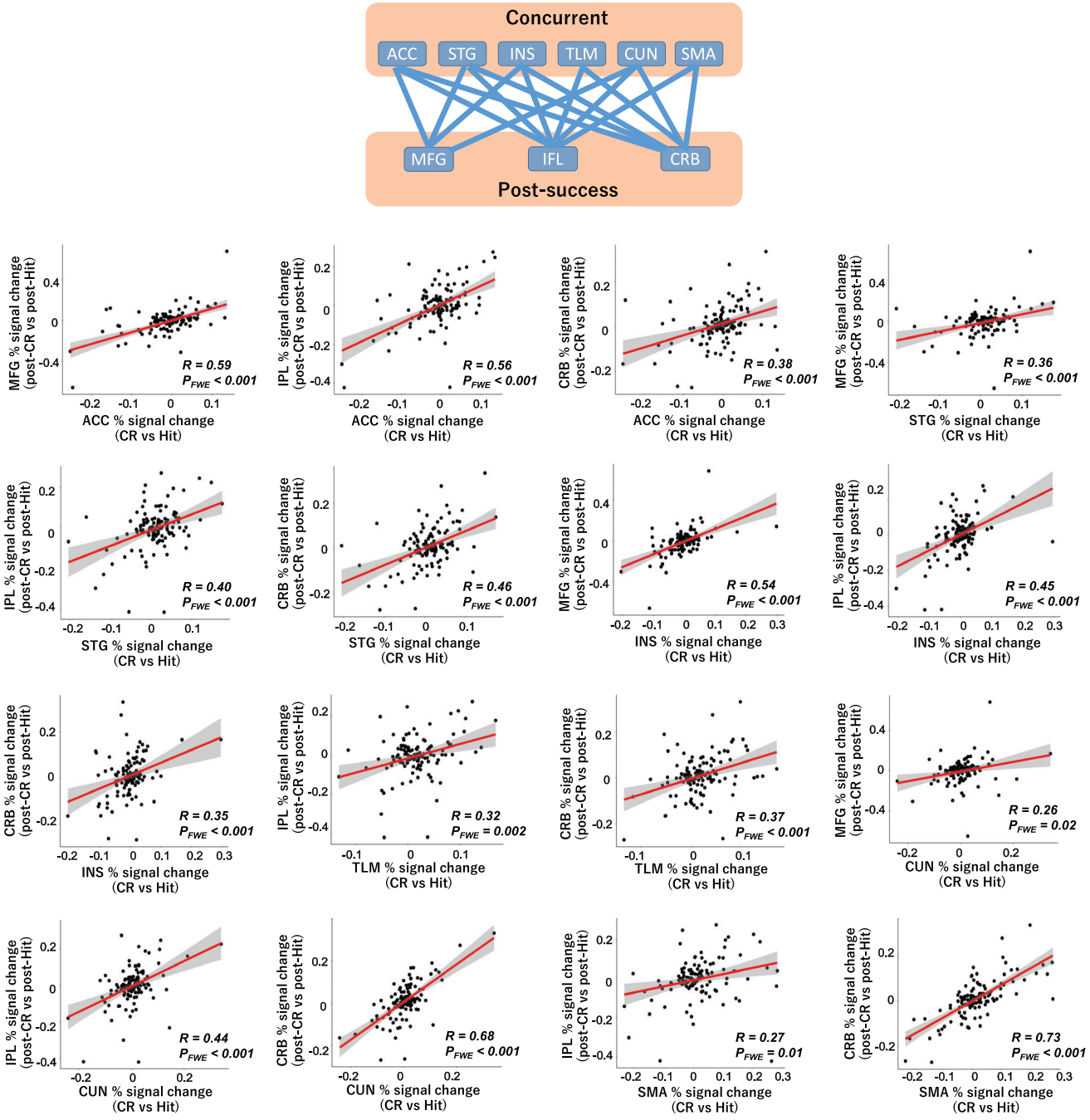

FIGURE 2 Associations between concurrent and poststop activations for correct cognitive control (i.e., CR and post-CR). Signal changes in concurrently activated regions significantly predicted signal changes in three postactivated regions. ACC, anterior cingulate cortex; CRB, cerebellum; CUN, cuneus; INS, insula; IPL, inferior parietal lobule; MFG, middle frontal gyrus; SMA, supplementary motor area; STG, superior temporal gyrus; TLM, thalamus

in the cingulo-opercular and fronto-parietal networks (Carter & van Veen, 2007; Kerns et al., 2004; MacDonald 3rd et al., 2000). Highly parallel to this hypothesis, our work has provided direct evidence that the two cognitive networks can be separated along the timeline of a stop-signal task, in which the cingulo-opercular network is specifically involved in concurrent performance monitoring and fronto-parietal network is specifically involved in poststop performance monitoring. This suggests that processing of cognitive control in humans is associated with two distinct neural systems with temporally different roles. Notably, this observation agrees strikingly well with current knowledge on the function of these two networks (Dosenbach et al., 2006; Dosenbach et al., 2007; Dosenbach et al., 2008). In particular, the cingulo-opercular network is considered to be critical in maintaining and stabilizing ongoing tasks in order to reach goal-directed behaviors, while the fronto-parietal network plays a pivotal role in initiating and adapting behaviors on a trial-to-trial basis in order

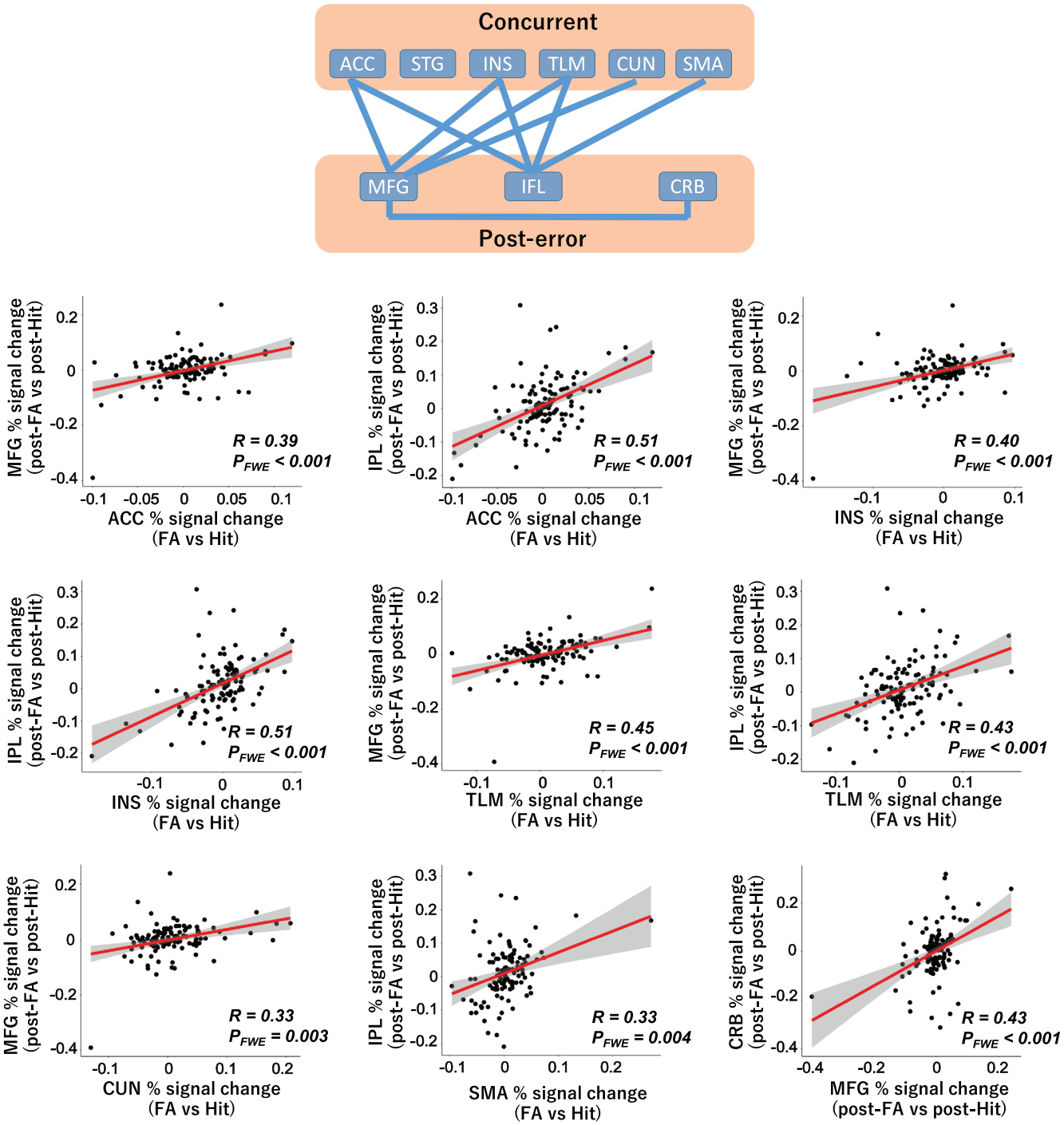

FIGURE 3 Associations between concurrent and poststop activations for incorrect cognitive control (i.e., FA and post-FA). Signal changes in concurrently activated regions significantly predicted signal changes in the prefrontal and parietal cortices but not cerebellum. Instead, posterror signal changes in the prefrontal cortex were significantly correlated with those in the cerebellum. ACC, anterior cingulate cortex; CRB, cerebellum; CUN, cuneus; INS, insula; IPL, inferior parietal lobule; MFG, middle frontal gyrus; SMA, supplementary motor area; STG, superior temporal gyrus; TLM, thalamus

to adjust performance. Therefore, the activation of cingulo-opercular network during concurrent performance monitoring is likely to reflect neural basis of conflict detection and the engagement of attentional effort to sustain and complete the ongoing trials, while the activation of fronto-parietal network during poststop performance monitoring may relate to corresponding adjustments of behavior for prior conflicts and the preparation of upcoming conflict trials.

Besides these two systems, several other regions that are not traditionally considered as part of these cognitive networks were also activated during the task, including the secondary motor areas, STG,

(a)

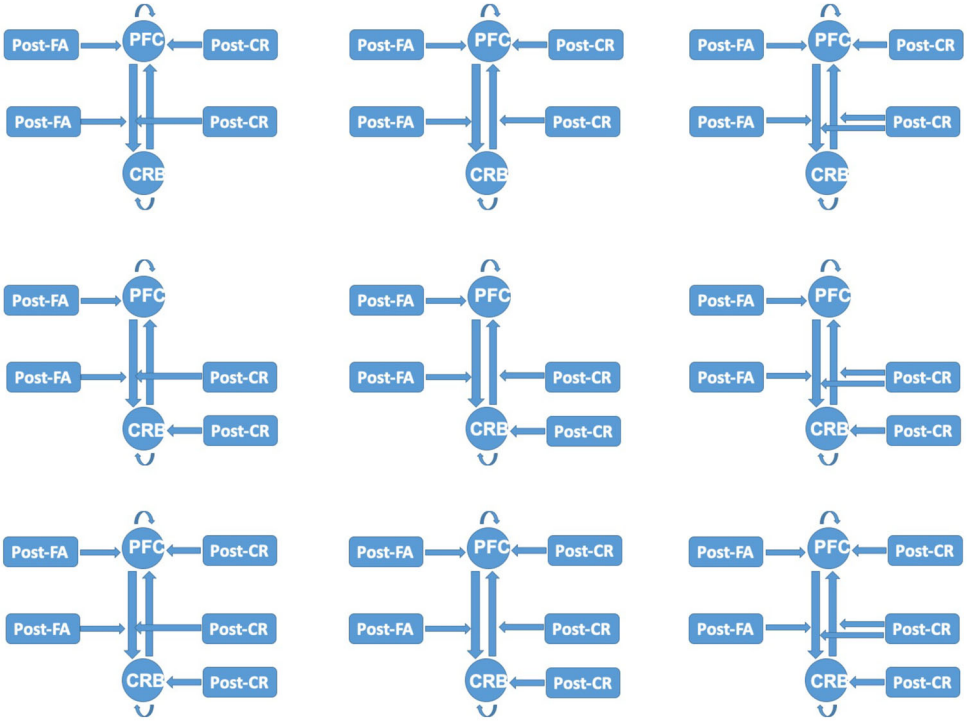

(b)

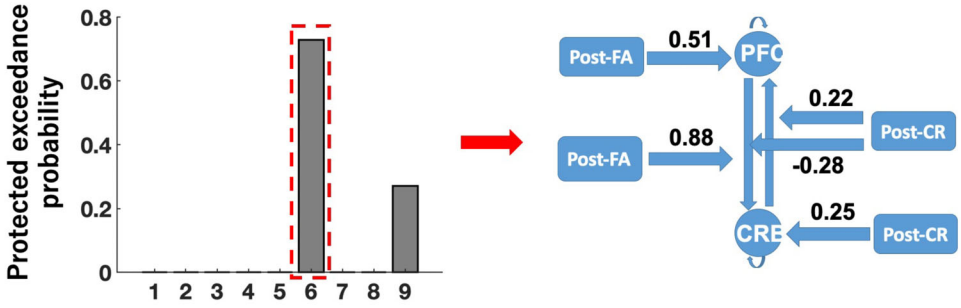

(c)

	Post-CR	Post-FA	P_{FWE}
Intrinsic connectivity			
PFC -> CRB		0.10±0.14	<0.001
CRB -> PFC		0.09±0.20	<0.001
Driving inputs			
PFC	-	0.51±0.31	<0.001
CRB	0.25±0.41	-	<0.001
Modulatory effects			
PFC -> CRB	-0.28±0.92	0.88±0.95	<0.001
CRB -> PFC	0.22±1.03	-	-

FIGURE 4 Dynamic causal modeling analysis for prefrontal-cerebellar connectivity during poststop cognitive control. (a) Illustration for the examined models in the DCM analysis. For posterror cognitive control (post-FA), driving input was fixed to the prefrontal cortex and modularity effect was fixed on top-down connectivity from the prefrontal cortex to cerebellum, based on correlation results shown in Figure 3. For postsuccess cognitive control (post-CR), three possibilities were considered for driving input (i.e., input to prefrontal cortex, input to cerebellum, and input to both) and for modulatory effect (i.e., from prefrontal to cerebellar, from cerebellar to prefrontal, and both directions) separately, thereby generating a total of nine models. (b) The Bayesian model selection identified a winning model with driving input to cerebellum and modularity effects on both directions during post-CR. Notably, prefrontal → cerebellar connectivity was negatively modulated (inhibited) during post-CR but positively modulated (excited) during post-FA. (c) Group-level parameters (mean ± *SD*) for the winning model estimated by Bayesian model averaging. Note that for intrinsic connectivity and driving inputs, significance is based on whether the parameters are different from zero (one-sample *t* test); while for modularity effects, significance is based on whether they are different between post-CR and post-FA (paired *t* test)

and visual areas during concurrent cognitive control and the posterior cerebellum during poststop cognitive control. The secondary motor areas encompassing the premotor cortex and SMA are crucial in planning, programming, and initiating voluntary movements in humans (Goldberg, 2010). In terms of cognitive control, these areas serve an intermediate role connecting the dACC and primary motor cortex to facilitate motor responses guided by simultaneous detection of conflict or incongruent information (Li et al., 2008; Ridderinkhof, Ullsperger, Crone, & Nieuwenhuis, 2004; Swick & Turken, 2002). The dysconnectivity between dACC and SMA may contribute to disruptions in error-related negativity and in turn error monitoring performance (Ridderinkhof et al., 2004; Swick & Turken, 2002). As a result, the activation of secondary motor areas during concurrent cognitive control may signal an "initiation" or "inhibition" command to exert on the primary motor cortex based on the active inputs from dACC. The STG, cuneus, and lingual gyrus are key areas for auditory and visual perceptions in humans. The activation of these regions is considered to be related to an amplification of neural representations of task-relevant perceptual information, possibly due to the attentional modulation to boost salient stimuli for resolution of stop trials (Danielmeier, Eichele, Forstmann, Tittgemeyer, & Ullsperger, 2011; Egner & Hirsch, 2005; Li, Huang, Constable, & Sinha, 2006; Stewart, Shen, Sham, & Alain, 2020; S. Zhang & Li, 2012). The activation of cerebellum during poststop monitoring tracks well with its role as an "error processing hub" of the brain. In particular, the cerebellar Purkinje cells receive and integrate information coming from the cerebral cortex, encode mismatch and errors in the received information, modify their firing rates, and elicit bottom-up projections to convey corrected signals back to the cerebrum (Diedrichsen, King, Hernandez-Castillo, Sereno, & Ivry, 2019; Herzfeld, Kojima, Soetedjo, & Shadmehr, 2018; Kostadinov, Beau, Blanco-Pozo, & Hausser, 2019; Schmahmann, 2019). Therefore, the activation of cerebellum during poststop but not concurrent cognitive control may suggest its specific function in resolving conflicts and adjusting behaviors.

Our findings showing that concurrent activations significantly predicted poststop activations in the lPFC and IPL during both correct and incorrect responses are broadly consistent with the conflict theory (Carter & van Veen, 2007). These results not only support the previous hypothesis that the activation of dACC detects incongruent information and further recruits the lPFC to resolve conflicts (Kerns et al., 2004; MacDonald 3rd et al., 2000), but also extend the hypothesis to a broader set of regions covering the cingulo-opercular and fronto-parietal networks. Beyond the traditionally focused dACC and lPFC, it is likely that the activations in the cingulo-opercular network generally serve as a guide signal to recruit the fronto-parietal network during poststop trials, and such mechanism is likely to be involved in both correct cognitive control and error processing.

Intriguingly, the cerebellum appears to be a major region whose poststop activation is differentially correlated with activations of concurrent performance monitoring between correct and incorrect responses, suggesting distinct neural mechanisms underlying the processing of correct and erroneous information in the cerebellum. Importantly, the results suggest that the cerebellar activation during poststop monitoring is likely to be driven by two competing systems depending on the involved situation. In case of correct response, the cerebellar is primarily activated by the preceding activations in the cingulo-opercular network, while the connectivity from the lPFC to cerebellum is inhibited. This may facilitate the consistency of ongoing behaviors and stabilize task response given prior success. In contrast, in case of erroneous response, the input from the cingulo-opercular network is diminished while the connectivity from the lPFC to cerebellum is excited. This may convey a top-down error signal instructing the cerebellum for error correction and behavioral adjustment. Together, these observations may suggest competitive top-down controls between the cingulo-opercular network and fronto-parietal network over the cerebellum, in order to achieve a functional balance for maintaining stability and flexibility of cognitive behaviors (Dosenbach et al., 2007, 2008). These observations are also consistent with the proposed theory of the cerebellum as a supervised learning system whose function is guided by signal inputs from the cerebral cortex (Doya, 2000; Ramnani, 2014).

It should be noted that, while cognitive control includes multiple cognitive components and can be examined with a variety of tasks and multiple imaging modalities, the results of this study are based on a particular fMRI stop-signal task. Thus, it would be useful to examine generalizability of the findings in other studies with different task paradigms and imaging modalities. For instance, neural signals related to conflict-related cognitive monitoring have been demonstrated to be affected by conflict frequency and intensity during the task (M. Botvinick, Nystrom, Fissell, Carter, & Cohen, 1999; Braver, Barch, Gray, Molfese, & Snyder, 2001; Jones, Cho, Nystrom, Cohen, & Braver, 2002; Nieuwenhuis, Yeung, van den Wildenberg, & Ridderinkhof, 2003). Since these factors are fixed and cannot be evaluated in the present study, our results may to certain degree be limited by the employed experimental parameters.

To sum up, the present data extend the previous findings in cognitive control by showing temporally separable and associated mechanisms underlying concurrent, postsuccess, and posterror performance monitoring in humans. While the findings still merit replication in future studies, these results provide initial evidence for the differential roles of cognitive control regions in subserving goal-directed behaviors. In addition, given common dysfunction of the cognitive control networks and cerebellum cross psychiatric disorders (H. Cao et al., 2018; Elliott, Romer, Knodt, & Hariri, 2018; Sha, Wager, Mechelli, & He, 2019; Shanmugan et al., 2016), these findings may also offer some useful implications for clinical research, and may help better interpret identified neural changes in patients and refine behavioral correlates of neuropathology among illnesses.

ACKNOWLEDGMENTS

This work was supported by the Brain and Behavior Research Foundation NARSAD Young Investigator Grant (No. 27068) to Dr. Cao. The authors would like to acknowledge the two anonymous reviewers for their valuable suggestions on this work.

CONFLICT OF INTEREST

Dr. Cannon has served as a consultant for Boehringer-Ingelheim Pharmaceuticals and Biogen. Dr. Cao reports no conflicts of interest.

DATA AVAILABILITY STATEMENT

The data used in this study are publicly available at https://openneuro.org/datasets/ds000030.

ORCID

Hengyi Cao https://orcid.org/0000-0003-4168-0391
Tyrone D. Cannon https://orcid.org/0000-0002-5632-3154

REFERENCES

Anticevic, A., Hu, S., Zhang, S., Savic, A., Billingslea, E., Wasylink, S., … Pittenger, C. (2014). Global resting-state functional magnetic resonance imaging analysis identifies frontal cortex, striatal, and cerebellar dysconnectivity in obsessive-compulsive disorder. *Biological Psychiatry*, *75*(8), 595–605. https://doi.org/10.1016/j.biopsych.2013.10.021

Becerril, K. E., & Barch, D. M. (2013). Conflict and error processing in an extended cingulo-opercular and cerebellar network in schizophrenia. *NeuroImage: Clinical*, *3*, 470–480. https://doi.org/10.1016/j.nicl.2013.09.012

Botvinick, M., Nystrom, L. E., Fissell, K., Carter, C. S., & Cohen, J. D. (1999). Conflict monitoring versus selection-for-action in anterior cingulate cortex. *Nature*, *402*(6758), 179–181. https://doi.org/10.1038/46035

Botvinick, M. M., Cohen, J. D., & Carter, C. S. (2004). Conflict monitoring and anterior cingulate cortex: An update. *Trends in Cognitive Sciences*, *8*(12), 539–546. https://doi.org/10.1016/j.tics.2004.10.003

Braver, T. S., Barch, D. M., Gray, J. R., Molfese, D. L., & Snyder, A. (2001). Anterior cingulate cortex and response conflict: Effects of frequency, inhibition and errors. *Cereb Cortex*, *11*(9), 825–836. https://doi.org/10.1093/cercor/11.9.825

Cao, H., & Cannon, T. (2019). Cerebellar dysfunction and schizophrenia: From "cognitive Dysmetria" to a potential therapeutic target. *American Journal of Psychiatry*, *176*(7), 498–500. https://doi.org/10.1176/appi.ajp.2019.19050480

Cao, H., Chen, O. Y., Chung, Y., Forsyth, J. K., McEwen, S. C., Gee, D. G., … Cannon, T. D. (2018). Cerebello-thalamo-cortical hyperconnectivity as a state-independent functional neural signature for psychosis prediction and characterization. *Nature Communications*, *9*(1), 3836. https://doi.org/10.1038/s41467-018-06350-7

Cao, H., McEwen, S. C., Chung, Y., Chen, O. Y., Bearden, C. E., Addington, J., … Cannon, T. D. (2019). Altered brain activation during memory retrieval precedes and predicts conversion to psychosis in individuals at clinical high risk. *Schizophrenia Bulletin*, *45*(4), 924–933. https://doi.org/10.1093/schbul/sby122

Carlisi, C. O., Norman, L., Murphy, C. M., Christakou, A., Chantiluke, K., Giampietro, V., … Rubia, K. (2017). Disorder-specific and shared brain abnormalities during vigilance in autism and obsessive-compulsive disorder. *Biological Psychiatry: Cognitive Neuroscience and Neuroimaging*, *2*(8), 644–654. https://doi.org/10.1016/j.bpsc.2016.12.005

Carter, C. S., Braver, T. S., Barch, D. M., Botvinick, M. M., Noll, D., & Cohen, J. D. (1998). Anterior cingulate cortex, error detection, and the online monitoring of performance. *Science*, *280*(5364), 747–749. https://doi.org/10.1126/science.280.5364.747

Carter, C. S., & van Veen, V. (2007). Anterior cingulate cortex and conflict detection: An update of theory and data. *Cognitive, Affective, & Behavioral Neuroscience*, *7*(4), 367–379. https://doi.org/10.3758/cabn.7.4.367

Danielmeier, C., Eichele, T., Forstmann, B. U., Tittgemeyer, M., & Ullsperger, M. (2011). Posterior medial frontal cortex activity predicts post-error adaptations in task-related visual and motor areas. *The Journal of Neuroscience*, *31*(5), 1780–1789. https://doi.org/10.1523/JNEUROSCI.4299-10.2011

Diedrichsen, J., King, M., Hernandez-Castillo, C., Sereno, M., & Ivry, R. B. (2019). Universal transform or multiple functionality? Understanding the contribution of the human cerebellum across task domains. *Neuron*, *102*(5), 918–928. https://doi.org/10.1016/j.neuron.2019.04.021

Dosenbach, N. U., Fair, D. A., Cohen, A. L., Schlaggar, B. L., & Petersen, S. E. (2008). A dual-networks architecture of top-down control. *Trends in Cognitive Sciences*, *12*(3), 99–105. https://doi.org/10.1016/j.tics.2008.01.001

Dosenbach, N. U., Fair, D. A., Miezin, F. M., Cohen, A. L., Wenger, K. K., Dosenbach, R. A., … Petersen, S. E. (2007). Distinct brain networks for adaptive and stable task control in humans. *Proceedings of the National Academy of Sciences of the United States of America*, *104*(26), 11073–11078. https://doi.org/10.1073/pnas.0704320104

Dosenbach, N. U., Visscher, K. M., Palmer, E. D., Miezin, F. M., Wenger, K. K., Kang, H. C., … Petersen, S. E. (2006). A core system for the implementation of task sets. *Neuron*, *50*(5), 799–812. https://doi.org/10.1016/j.neuron.2006.04.031

Doya, K. (2000). Complementary roles of basal ganglia and cerebellum in learning and motor control. *Current Opinion in Neurobiology*, *10*(6), 732–739. https://doi.org/10.1016/s0959-4388(00)00153-7

Duan, K., Chen, J., Calhoun, V. D., Lin, D., Jiang, W., Franke, B., … Liu, J. (2018). Neural correlates of cognitive function and symptoms in attention-deficit/hyperactivity disorder in adults. *NeuroImage: Clinical*, *19*, 374–383. https://doi.org/10.1016/j.nicl.2018.04.035

Egner, T., & Hirsch, J. (2005). Cognitive control mechanisms resolve conflict through cortical amplification of task-relevant information. *Nature Neuroscience*, *8*(12), 1784–1790. https://doi.org/10.1038/nn1594

Elliott, M. L., Romer, A., Knodt, A. R., & Hariri, A. R. (2018). A Connectome-wide functional signature of transdiagnostic risk for mental illness. *Biological Psychiatry*, *84*(6), 452–459. https://doi.org/10.1016/j.biopsych.2018.03.012

Friston, K. J., Harrison, L., & Penny, W. (2003). Dynamic causal modelling. *NeuroImage*, *19*(4), 1273–1302. https://doi.org/10.1016/s1053-8119(03)00202-7

Garavan, H., Ross, T. J., Kaufman, J., & Stein, E. A. (2003). A midline dissociation between error-processing and response-conflict monitoring. *NeuroImage*, *20*(2), 1132–1139. https://doi.org/10.1016/S1053-8119(03)00334-3

Garavan, H., Ross, T. J., Murphy, K., Roche, R. A., & Stein, E. A. (2002). Dissociable executive functions in the dynamic control of behavior: Inhibition, error detection, and correction. *Neuroimage*, *17*(4) 1820-1829, 1820–1829. https://doi.org/10.1006/nimg.2002.1326

Goldberg, G. (2010). Supplementary motor area structure and function: Review and hypotheses. *Behavioral and Brain Sciences*, *8*(4), 567–588. https://doi.org/10.1017/S0140525X00045167

Gorgolewski, K. J., Durnez, J., & Poldrack, R. A. (2017). Preprocessed consortium for neuropsychiatric phenomics dataset. *F1000Res*, *6*, 1262. https://doi.org/10.12688/f1000research.11964.2

Hendrick, O. M., Ide, J. S., Luo, X., & Li, C. S. (2010). Dissociable processes of cognitive control during error and non-error conflicts: A study of the stop signal task. *PLoS One*, *5*(10), e13155. https://doi.org/10.1371/journal.pone.0013155

Herzfeld, D. J., Kojima, Y., Soetedjo, R., & Shadmehr, R. (2018). Encoding of error and learning to correct that error by the Purkinje cells of the cerebellum. *Nature Neuroscience*, *21*(5), 736–743. https://doi.org/10.1038/s41593-018-0136-y

Ide, J. S., & Li, C. S. (2011). A cerebellar thalamic cortical circuit for error-related cognitive control. *NeuroImage*, *54*(1), 455–464. https://doi.org/10.1016/j.neuroimage.2010.07.042

Ito, H., Mori, K., Harada, M., Hisaoka, S., Toda, Y., Mori, T., … Kagami, S. (2017). A proton magnetic resonance spectroscopic study in autism Spectrum disorder using a 3-tesla clinical magnetic resonance imaging (MRI) system: The anterior cingulate cortex and the left cerebellum.

Journal of Child Neurology, *32*(8), 731–739. https://doi.org/10.1177/0883073817702981

Ji, J. L., Spronk, M., Kulkarni, K., Repovš, G., Anticevic, A., & Cole, M. W. (2019). Mapping the human brain's cortical-subcortical functional network organization. *NeuroImage*, *185*, 35–57. https://doi.org/10.1016/j.neuroimage.2018.10.006

Jones, A. D., Cho, R. Y., Nystrom, L. E., Cohen, J. D., & Braver, T. S. (2002). A computational model of anterior cingulate function in speeded response tasks: Effects of frequency, sequence, and conflict. *Cognitive, Affective, & Behavioral Neuroscience*, *2*(4), 300–317. https://doi.org/10.3758/cabn.2.4.300

Kerns, J. G., Cohen, J. D., MacDonald, A. W., 3rd, Cho, R. Y., Stenger, V. A., & Carter, C. S. (2004). Anterior cingulate conflict monitoring and adjustments in control. *Science*, *303*(5660), 1023–1026. https://doi.org/10.1126/science.1089910

Kostadinov, D., Beau, M., Blanco-Pozo, M., & Hausser, M. (2019). Predictive and reactive reward signals conveyed by climbing fiber inputs to cerebellar Purkinje cells. *Nature Neuroscience*, *22*(6), 950–962. https://doi.org/10.1038/s41593-019-0381-8

Li, C. S., Huang, C., Constable, R. T., & Sinha, R. (2006). Imaging response inhibition in a stop-signal task: Neural correlates independent of signal monitoring and post-response processing. *The Journal of Neuroscience*, *26*(1), 186–192. https://doi.org/10.1523/JNEUROSCI.3741-05.2006

Li, C. S., Yan, P., Chao, H. H., Sinha, R., Paliwal, P., Constable, R. T., … Lee, T. W. (2008). Error-specific medial cortical and subcortical activity during the stop signal task: A functional magnetic resonance imaging study. *Neuroscience*, *155*(4), 1142–1151. https://doi.org/10.1016/j.neuroscience.2008.06.062

Lynch, C. J., Breeden, A. L., You, X., Ludlum, R., Gaillard, W. D., Kenworthy, L., & Vaidya, C. J. (2017). Executive dysfunction in autism spectrum disorder is associated with a failure to modulate frontoparietal-insular hub architecture. *Biological Psychiatry: Cognitive Neuroscience and Neuroimaging*, *2*(6), 537–545. https://doi.org/10.1016/j.bpsc.2017.03.008

MacDonald, A. W., 3rd, Cohen, J. D., Stenger, V. A., & Carter, C. S. (2000). Dissociating the role of the dorsolateral prefrontal and anterior cingulate cortex in cognitive control. *Science*, *288*(5472), 1835–1838. https://doi.org/10.1126/science.288.5472.1835

Mathalon, D. H., Whitfield, S. L., & Ford, J. M. (2003). Anatomy of an error: ERP and fMRI. *Biological Psychology*, *64*(1–2), 119–141. https://doi.org/10.1016/s0301-0511(03)00105-4

Menon, V., Adleman, N. E., White, C. D., Glover, G. H., & Reiss, A. L. (2001). Error-related brain activation during a Go/NoGo response inhibition task. *Human Brain Mapping*, *12*(3), 131–143. https://doi.org/10.1002/1097-0193(200103)12:3<131::aid-hbm1010>3.0.co;2-c

Mostert, J. C., Shumskaya, E., Mennes, M., Onnink, A. M., Hoogman, M., Kan, C. C., … Norris, D. G. (2016). Characterising resting-state functional connectivity in a large sample of adults with ADHD. *Progress in Neuro-Psychopharmacology & Biological Psychiatry*, *67*, 82–91. https://doi.org/10.1016/j.pnpbp.2016.01.011

Nieuwenhuis, S., Yeung, N., van den Wildenberg, W., & Ridderinkhof, K. R. (2003). Electrophysiological correlates of anterior cingulate function in a go/no-go task: Effects of response conflict and trial type frequency. *Cognitive, Affective, & Behavioral Neuroscience*, *3*(1), 17–26. https://doi.org/10.3758/CABN.3.1.17

Penny, W. D., Stephan, K. E., Daunizeau, J., Rosa, M. J., Friston, K. J., Schofield, T. M., & Leff, A. P. (2010). Comparing families of dynamic causal models. *PLoS Computational Biology*, *6*(3), e1000709. https://doi.org/10.1371/journal.pcbi.1000709

Poldrack, R. A., Congdon, E., Triplett, W., Gorgolewski, K. J., Karlsgodt, K. H., Mumford, J. A., … Bilder, R. M. (2016). A phenome-wide examination of neural and cognitive function. *Scientific Data*, *3*, 160110. https://doi.org/10.1038/sdata.2016.110

Power, J. D., Mitra, A., Laumann, T. O., Snyder, A. Z., Schlaggar, B. L., & Petersen, S. E. (2014). Methods to detect, characterize, and remove motion artifact in resting state fMRI. *NeuroImage*, *84*, 320–341. https://doi.org/10.1016/j.neuroimage.2013.08.048

Ramnani, N. (2014). Automatic and controlled processing in the corticocerebellar system. *Progress in Brain Research*, *210*, 255–285. https://doi.org/10.1016/b978-0-444-63356-9.00010-8

Ridderinkhof, K. R., Ullsperger, M., Crone, E. A., & Nieuwenhuis, S. (2004). The role of the medial frontal cortex in cognitive control. *Science*, *306*(5695), 443–447. https://doi.org/10.1126/science.1100301

Rigoux, L., Stephan, K. E., Friston, K. J., & Daunizeau, J. (2014). Bayesian model selection for group studies - revisited. *NeuroImage*, *84*, 971–985. https://doi.org/10.1016/j.neuroimage.2013.08.065

Schmahmann, J. D. (2019). The cerebellum and cognition. *Neuroscience Letters*, *688*, 62–75. https://doi.org/10.1016/j.neulet.2018.07.005

Sha, Z., Edmiston, E. K., Versace, A., Fournier, J. C., Graur, S., Greenberg, T., … Phillips, M. L. (2020). Functional disruption of cerebello-thalamo-cortical networks in obsessive-compulsive disorder. *Biological Psychiatry: Cognitive Neuroscience and Neuroimaging*, *5*(4), 438–447. https://doi.org/10.1016/j.bpsc.2019.12.002

Sha, Z., Wager, T. D., Mechelli, A., & He, Y. (2019). Common dysfunction of large-scale neurocognitive networks across psychiatric disorders. *Biological Psychiatry*, *85*(5), 379–388. https://doi.org/10.1016/j.biopsych.2018.11.011

Shanmugan, S., Wolf, D. H., Calkins, M. E., Moore, T. M., Ruparel, K., Hopson, R. D., … Satterthwaite, T. D. (2016). Common and dissociable mechanisms of executive system dysfunction across psychiatric disorders in youth. *The American Journal of Psychiatry*, *173*(5), 517–526. https://doi.org/10.1176/appi.ajp.2015.15060725

Stephan, K. E., Penny, W. D., Daunizeau, J., Moran, R. J., & Friston, K. J. (2009). Bayesian model selection for group studies. *NeuroImage*, *46*(4), 1004–1017. https://doi.org/10.1016/j.neuroimage.2009.03.025

Stephan, K. E., Penny, W. D., Moran, R. J., den Ouden, H. E., Daunizeau, J., & Friston, K. J. (2010). Ten simple rules for dynamic causal modeling. *NeuroImage*, *49*(4), 3099–3109. https://doi.org/10.1016/j.neuroimage.2009.11.015

Stewart, H. J., Shen, D., Sham, N., & Alain, C. (2020). Involuntary orienting and conflict resolution during auditory attention: The role of ventral and dorsal streams. *Journal of Cognitive Neuroscience*, *32*, 1–13. https://doi.org/10.1162/jocn_a_01594

Swick, D., & Turken, U. (2002). Dissociation between conflict detection and error monitoring in the human anterior cingulate cortex. *Proceedings of the National Academy of Sciences*, *99*(25), 16354–16359. https://doi.org/10.1073/pnas.252521499

Taylor, S. F., Stern, E. R., & Gehring, W. J. (2007). Neural systems for error monitoring: Recent findings and theoretical perspectives. *The Neuroscientist*, *13*(2), 160–172. https://doi.org/10.1177/1073858406298184

Zeidman, P., Jafarian, A., Corbin, N., Seghier, M. L., Razi, A., Price, C. J., & Friston, K. J. (2019). A guide to group effective connectivity analysis, part 1: First level analysis with DCM for fMRI. *NeuroImage*, *200*, 174–190. https://doi.org/10.1016/j.neuroimage.2019.06.031

Zhang, S., & Li, C. S. (2012). Functional networks for cognitive control in a stop signal task: Independent component analysis. *Human Brain Mapping*, *33*(1), 89–104. https://doi.org/10.1002/hbm.21197

Zhang, Y., Ide, J. S., Zhang, S., Hu, S., Valchev, N. S., Tang, X., & Li, C. R. (2017). Distinct neural processes support post-success and post-error slowing in the stop signal task. *Neuroscience*, *357*, 273–284. https://doi.org/10.1016/j.neuroscience.2017.06.011

How to cite this article: Cao H, Cannon TD. Distinct and temporally associated neural mechanisms underlying concurrent, postsuccess, and posterror cognitive controls: Evidence from a stop-signal task. *Hum Brain Mapp*. 2021;42:2677–2690. https://doi.org/10.1002/hbm.25347